Defect formation in H implantation of crystalline Si

J. Keinonen, M. Hautala, E. Rauhala, V. Karttunen, A. Kuronen, and J. Räisänen
Accelerator Laboratory, University of Helsinki, Hämeentie 100, SF-00550 Helsinki 55, Finland

J. Lahtinen, A. Vehanen, E. Punkka, and P. Hautojärvi
Laboratory of Physics, Helsinki University of Technology, SF-02150 Espoo 15, Finland
(Received 21 October 1987)

The distributions of H atoms, displaced Si atoms, and vacancy-type defects in Si(100) produced by the implantation, at room temperature, of 1×10^{16} 35-, 60-, and 100-keV H^+-ions/cm^2 were measured with use of ion and slow-positron beam techniques. Three different regions of damage were observed. The damage distribution did not correlate with the deposited energy distribution. A vacancy-type damage region surviving room-temperature annealing and the dynamic annealing during implantation is produced in the region where the energy of the primary Si recoils exceeds a threshold value of 2.0 ± 0.5 keV, i.e., an energy spike is needed for damage formation. In the region of the deposited energy peak, H is associated with damage consisting of SiH centers and vacancy complexes. At the end region of the implantation range, the distribution of displaced Si atoms is produced by H impurities in crystalline Si. Two different recovery stages were observed. The first stage, at 500 K, is associated with the damage region containing vacancy-type defects and SiH centers with vacancy complexes; the recovery energy is 1.7 eV. The second stage, at 700 K, is attributed to the end region of the H range, where the recovery energy associated with the recrystallization of Si after the H loss is 2.1 eV.

I. INTRODUCTION

The processes which generate damage in crystalline silicon (*c*-Si) during ion bombardment have been studied extensively for over two decades (e.g., Refs. 1–6 and references therein). The slowing down of an energetic ion produces a cascade of atomic displacements in *c*-Si, resulting in damage and, ultimately an amorphous zone around the implantation track. As several implantation variables (temperature, flux, fluence, ion mass, and energy) are involved, however, there is some controversy about the mechanisms by which a cascade of atomic displacements results in damage.[7–9]

In this study, we combined three different techniques to study H-implantation-induced damage in *c*-Si and measured the distributions of vacancy-type defects with slow positrons, H atoms with the nuclear resonance broadening (NRB) method,[10] and Si atoms displaced from the lattice site (Si_D) with the Rutherford backscattering spectroscopy (RBS) and channeling. Based on the distributions in the room-temperature implanted *c*-Si and the observed recovery stages of the defects, a new interpretation is given to damage induced in *c*-Si by ion bombardment. We have briefly presented this interpretation earlier.[10] This work completes the technical aspects of the measurements and analysis, and the inclusion of new results allows a more detailed interpretation.

II. EXPERIMENTAL ARRANGEMENTS

The samples were prepared at the University of Helsinki 100-kV isotope separator by implanting 1×10^{16} 35-, 60-, and 100-keV H^+-ions/cm^2 into *n*-type Si(100) slices at room temperature. The incident H^+ beam was normal to the (100) face, with an intensity of 0.4 μA/cm^2. To ensure the lateral homogeneity of the samples, the implantation was performed with a two-directional sweeping system, which produces an overall homogeneity of within 1% for an implanted area of 10×20 mm^2.

The recovery of different defects was studied using 60-min isochronal annealings. To be able to follow the evolution of H and Si_D concentration profiles, the annealings were carried out in a quartz-tube furnace, in a low-pressure dry argon atmosphere of less than 50 μPa. The temperatures 500–1000 K of the samples were measured with a calibrated Chromel-Alumel thermocouple in close contact with the sample. In the slow-positron measurements, the annealings from 300 to 1200 K were performed *in situ*, in an ultrahigh-vacuum (UHV) chamber with a pressure of about 10 nPa. The temperatures were measured with a thermocouple gauge.

The depth profiling of implanted H atoms was carried out by the NRB technique, using a $^{15}N^{+2}$ beam from the University of Helsinki EGP-10-II tandem accelerator in conjunction with the 6.385-MeV resonance of the $^1H(^{15}N,\alpha\gamma)^{12}C$ reaction.[11] The depth resolution was about 10 nm at the surface. The beam intensity at the 3×3-mm^2 spot on the target was about 30-particle nA. The γ radiation was detected with two 12.7-cm-diam$\times$10.2-cm NaI(Tl) crystals.

The Si_D distributions were measured by RBS and channeling with 2.0-MeV $^4He^+$ ions from the University of Helsinki 2.5-MV Van de Graaff accelerator. Backscattered particles were analyzed with a 50-mm^2 Si(Li) detec-

tor located at 155° with respect to the incident beam at a distance of 65 mm from the target. The angular divergence of the incident beam was less than 0.02°. The samples were mounted on a precision goniometer, and the beam was aligned with respect to the ⟨100⟩ axis. The total accumulated ion charge per sample was always less than 35 μC. The relative ion doses for spectra from the ⟨100⟩-aligned virgin and damaged crystals as well as for the random-oriented spectra measured by tilting the goniometer about 6° away from the main channeling axis were obtained by using a beam chopper with a separate pulse analysis system having better than 2% accuracy.

The depth distributions of vacancy-type defects caused by the H^+-ion implantation were measured by using the slow-positron beam at the Helsinki University of Technology.[12] The sample was mounted in the UHV chamber, and a variable-energy (10–30-keV), monoenergetic ($\delta E \lesssim 3$-eV) positron beam (typically 10^6/sec) was made to strike the sample. The characteristics of the 511-keV positron annihilation radiation were recorded, with an HP Ge detector adjacent to the sample, as a function of incident beam energy. 2×10^6 counts were collected on the 511-keV annihilation line at each incident energy.

III. MEASUREMENTS AND RESULTS

The damage induced by hydrogen implantation was studied by taking measurements of the as-implanted and annealed samples.

A. Hydrogen distributions

In NRB profiling, the atomic fraction of hydrogen atoms f in a target composition $Si_{1-f}H_f$ was deduced by comparison of the γ-ray yield with that obtained from a H standard.[11]

The depth scale x was calculated from the successively increasing nitrogen-ion energies E_i, using the formulas

$$x(E_1)=\frac{E_1-E_r}{\varepsilon(E_1)}\ ,$$
$$x(E_i)=\frac{E_i-E_{i-1}}{0.5[\varepsilon(E_i)+\varepsilon(E_{i-1})]},\quad i\geq 2 \tag{1}$$

where E_i is the nitrogen beam energy of the ith point of measurement in keV, E_r is the resonance energy 6385 keV, and $\varepsilon(E_i)$ is the nitrogen stopping power (in units of keV/nm) of the mixture $Si_{1-f}H_f$. The commonly adopted stopping power value of 291 eV/10^{15} atoms-cm^2 was used for Si.[13,14] The Si density was assumed to be that of crystalline silicon. The stopping power for H was taken from Ref. 15.

The measured range profiles of the as-implanted samples and hydrogen distributions after annealings at different temperatures are shown in Fig. 1.

B. Si_D atom distributions

The number of Si_D atoms was determined following the conventional procedure.[16] The initially aligned beam traversing along a crystal axis may be divided into two components, the channeled and dechanneled parts. Dechanneling in a damaged crystal is mainly due to collisions of the ions with defects and, to a lesser degree, with lattice atoms. Scattering through angles larger than the critical angle results in deflection of part of the beam away from the channel. This dechanneled component encounters all atoms, and is backscattered as in amorphous material.

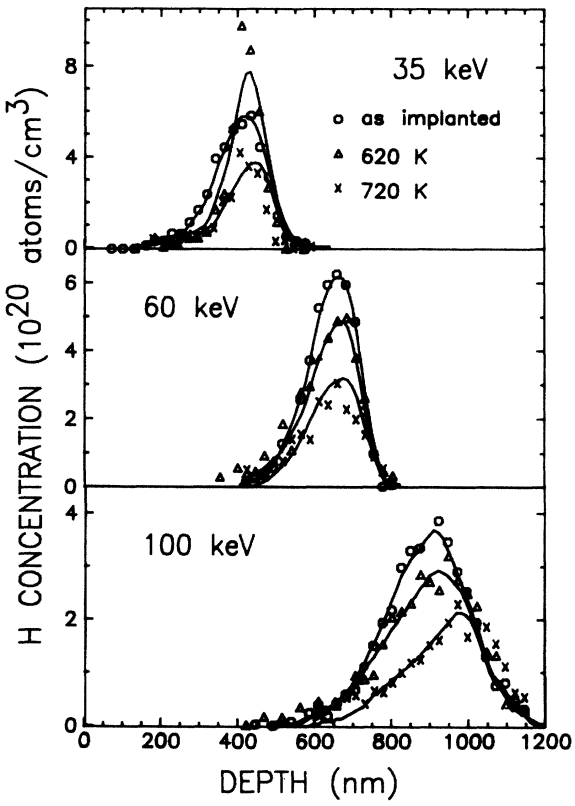

FIG. 1. Hydrogen distributions of the 1×10^{16} 35-, 60-, and 100-keV H^+-ions/cm^2 in c-Si. The solid lines through the measured points are the computer simulations of the range profiles. Hydrogen distributions after 60-min isochronal annealings are also shown. The solid lines are from the computer simulation of the annealing behavior of H (see the discussion).

The probability of dechanneling $P(x)$ caused by the displaced Si atoms located between the sample surface and depth x is proportional to the number of displaced atoms N_D (atoms/cm^3) and the cross section for dechanneling σ_D

$$P(x)=\sigma_D N_D x\ . \tag{2}$$

At the surface N_D is given by

$$N_D(0)=N\frac{\chi(0)-\chi_v(0)}{1-\chi_v(0)}\ , \tag{3}$$

where N is the bulk density of atoms, χ the experimentally determined ratio of aligned to random yields, and χ_v the ratio for the virgin crystal. At depth x the normalized yield is

$$\chi(x)=[1-\chi_D(x)]\frac{N_D(x)}{N}+\chi_D(x)\ , \tag{4}$$

where χ_D is the dechanneled fraction of the beam

$$\chi_D(x)=\chi_v(x)+[1-\chi_v(x)]P(x)\ . \tag{5}$$

For the calculation, the sample is assumed to be divided into thin slabs. The dechanneled fraction at depth x is given by Eqs. (2) and (5) from dechanneling by defects between the surface and depth x. Solving Eq. (4) then gives N_D in the next slab. The defect distribution as a function of depth is thus obtained. As the dechanneled fraction $\chi_D(x)$ should equal the aligned yield $\chi(x)$ below the disorder region, the whole procedure was iterated, varying the unknown cross section σ_D until this condition was fulfilled.

The stopping power from Ref. 17 with the 10%, 20%, and 20% reduction for the impinging channeled $^4He^+$ ions for the 35-, 60-, and 100-keV targets, respectively, yielded a depth scale in agreement with that obtained with the ^{15}N stopping.

The measured Si_D atom distributions in the as-implanted and annealed samples are shown in Fig. 2.

C. Vacancy distributions

After implantation, positrons rapidly thermalize in the solid sample and execute a diffusive motion.[18] The ability to detect vacancy-type lattice defects is based on the trapping of positrons at vacant lattice sites. Measurements of the shape of the 511-keV annihilation line can be used to distinguish between free and localized positrons as well as those diffused back to the sample surface. A characteristic parameter S, defined as the area of a fixed central region of the 511-keV line divided by the total area of the peak, is shown in Fig. 3 as a function of the incident positron energy E. While the data at small E is dominated by annihilations at the surface, the high-energy behavior of $S(E)$, both in irradiated and unirradiated Si(100) samples, is due to free-positron annihilations deep inside the samples. Differences in the two sets of data are ascribed to positrons annihilating in the vacancy-type defects produced by the 60-keV proton irradiation. The differences at $E=0$ are due to changes in the surface properties caused by irradiation, and they can be removed by scaling (see below).

We describe positron motion by the diffusion-annihilation equation[10,19,20]

$$D_+\nabla^2 n(x,E)-[\lambda_b+\mu C_{vac}(x)]n(x,E)+P(x,E)=0\ , \tag{6}$$

where D_+ is the positron diffusion coefficient, $n(x,E)$ the quasistationary positron density at the depth x for the incident positron energy E, λ_b the free-positron annihilation rate, μ the specific trapping rate, $C_{vac}(x)$ the vacancy concentration, and $P(x,E)$ the positron implantation profile. For the implantation profile we use[19,21]

$$P(x,E)=(2x/x_0^2)e^{-(x/x_0)^2}\ , \tag{7}$$

where

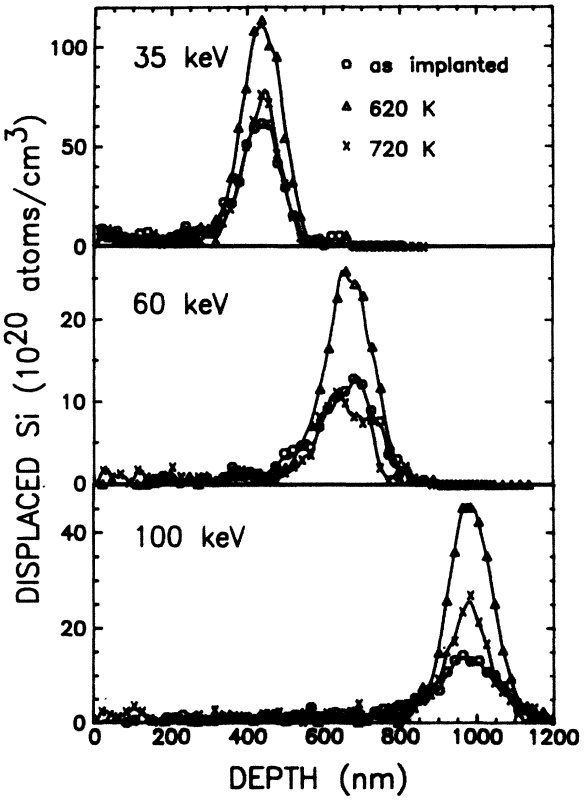

FIG. 2. Measured distributions of displaced Si atoms (Si_D) in as-implanted c-Si and after 60-min isochronal annealings. The solid lines through the data points are drawn to guide the eye.

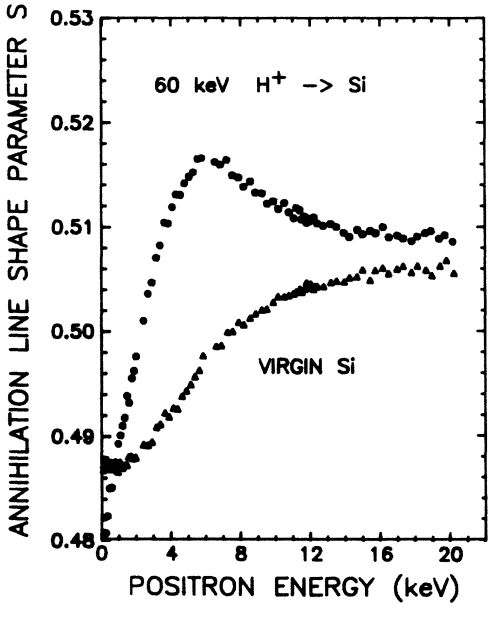

FIG. 3. Positron annihilation line-shape parameter S vs incident positron energy for the unimplanted c-Si and the corresponding 60-keV implanted sample.

$$x_0 = 18.6[E/(1\ \text{keV})]^{1.6}\ \text{nm} . \quad (8)$$

By solving this equation at each incident energy E, we can calculate the fraction of positrons annihilating at the surface

$$f_{\text{surf}}(E) = D_+ \nabla n(0,E) , \quad (9)$$

in the vacancies

$$f_{\text{vac}}(E) = \int_0^\infty dx\, \mu C_{\text{vac}}(x) n(x,E) , \quad (10)$$

and in the bulk

$$f_{\text{bulk}}(E) = \int_0^\infty dx\, \lambda_b n(x,E) . \quad (11)$$

The line-shape parameter $S(E)$ is then obtained as a superposition of the different annihilations from

$$S(E) = f_{\text{surf}}(E) S_{\text{surf}} + f_{\text{vac}}(E) S_{\text{vac}} + f_{\text{bulk}}(E) S_{\text{bulk}} . \quad (12)$$

To extract the spatial vacancy defect distribution, we vary $C_{\text{vac}}(x)$ and calculate $S(E)$ from Eqs. (6)–(12) until a satisfactory fit to the experimental $S_{\text{irr}}(E)$ curve is reached.

For better illustration of the changes caused by irradiation-induced defects, we consider[10,20] the difference data

$$\Delta S(E) = S_{\text{irr}}(E) - S_{\text{unirr}}(E) . \quad (13)$$

Because the surface properties, and thus the parameter S_{surf}, may change during irradiations and thermal annealings, for each sample we have scaled the $S_{\text{unirr}}(E)$ curves to correspond with the proper S_{surf} value so that $\Delta S(0) \approx 0$.

In the unirradiated sample, positron motion was well characterized by free diffusion with $D_+ = 2.9\ \text{cm}^2/\text{s}$. The diffusion-related parameter E_0 had a value of 5.1 keV, which is slightly higher than that reported earlier.[22] The characteristic values $S_{\text{surf}} = 0.4870$ and $S_{\text{bulk}} = 0.5075$ for the unirradiated sample were measured at $E = 0.1$ and 25 keV, respectively. As discussed earlier, the latter describes annihilations far behind the damaged region in all the samples. S_{surf} for irradiated samples varied from 0.48 to 0.51. A value $S_{\text{vac}} = 1.034 S_{\text{bulk}}$ was adopted to describe positron annihilation at H^+-irradiation-induced vacancy defects. This value was obtained from separate measurements of high-fluence (saturation positron trapping) 12-MeV Si^+-irradiated Si(100) samples.[23] We observed in the fitting that a change in S_{vac} causes a change in the total number of defects but not in the shape of the defect distributions. A value of $10^{14}\ \text{s}^{-1}$ was used for the specific trapping rate of vacancy defects (divacancies) in Si.[24] A satisfactory fit to the experimental data was obtained using a constant vacancy profile with a well-defined cutoff depth. The mean depth

$$\int_0^\infty dx\, x C_{\text{vac}}(x) \Big/ \int_0^\infty dx\, C_{\text{vac}}(x) \quad (14)$$

and the total-positron trapping rate

$$\int_0^\infty dx\, \mu C_{\text{vac}}(x) \quad (15)$$

have a statistical uncertainty of about 15%.

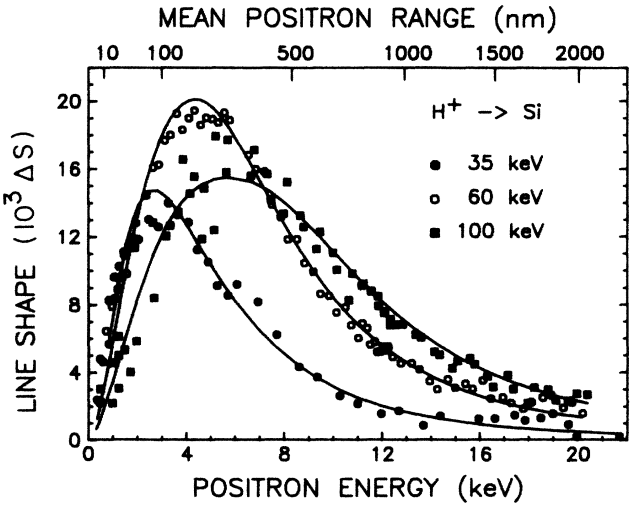

FIG. 4. Doppler-broadened annihilation line-shape data ΔS vs incident positron energy for the as-implanted 35-, 60-, and 100-keV samples. The solid lines are the fits corresponding to the vacancy profiles shown in Fig. 5.

The absolute scale of the number of defects depends on the choice of the value of S_{vac} and the specific trapping rate μ. We think the uncertainties in the concentration scales are less than a factor of 3.

The experimental and fitted annihilation line-shape data ΔS *versus* the incident positron energy E are shown in Fig. 4 for the as-implanted samples. The extracted vacancy complex distributions are displayed in Fig. 5. The annealing behavior of the vacancy-type defects are illustrated in Fig. 6 by the parameter ΔS. The extracted vacancy distribution parameters are given in Table I.

D. Results of annealings

The room-temperature irradiation of c-Si with neutrons[23] or ^{16}O (Refs. 25 and 26), ^{11}B, ^{64}Zn, and ^{121}Sb ions (Ref. 27) is known to yield the formation of divacancies

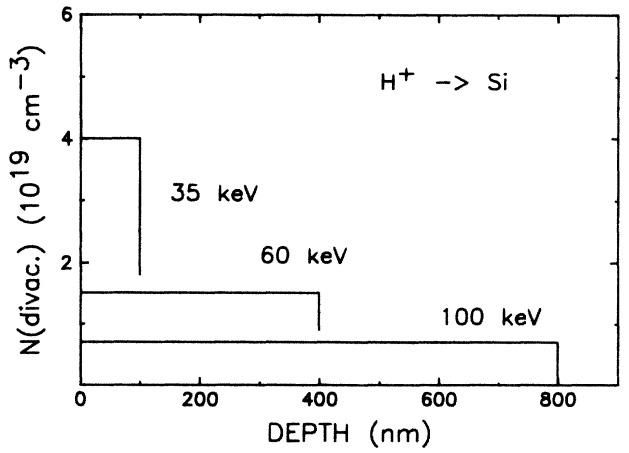

FIG. 5. Divacancy distributions due to the 1×10^{16} 35-, 60-, and 100-keV H^+-ions/cm^2 in c-Si.

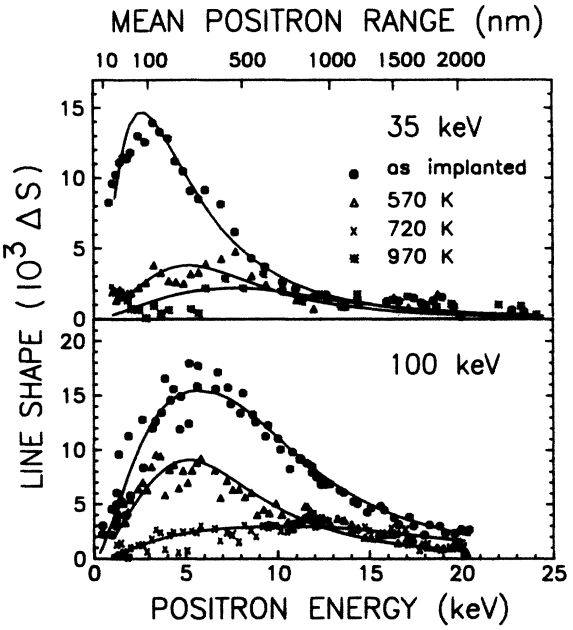

FIG. 6. Doppler-broadened annihilation line-shape data ΔS vs incident positron energy for the annealed samples. The solid lines are the fits corresponding to the vacancy profiles given in Table I.

as predominant vacancy defects. Divacancies are known to become mobile at 470–610 K.[2,25,28] We observed the abrupt annealing of vacancy-type defects in the regions 0–100 nm (the 35-keV implantation), 0–400 nm (60 keV), and 0–800 nm (100 keV) in the temperature region 470–570 K. This resulted in a reduction of the concentrations by about a factor of 10, and extension of the distributions to the depths 500 nm (35 keV) and 2000 nm (60 and 100 keV). In annealings above 900 K, continuous losses of vacancies and the broadening of the distribution lead to a defect-free state at about 1200 K. The annealing behavior of the total amount of the vacancy-type defects as well as of the hydrogen atoms are illustrated in Fig. 7.

In the regions around 350, 620, and 870 nm of the 35-, 60-, and 100-keV samples, respectively, where the peaks of the deposited energy distribution overlap with the H distribution, a rapid loss of H starts at about 570 K (Fig. 1). In these regions, only isolated Frenkel pairs are produced during the implantation. The association of vacancies with SiH centers has previously been postulated by Stein.[29] Our results support this interpretation.

The coupling of H and Si_D atom distributions have been demonstrated by earlier studies.[30] The constant, implantation energy independent width of the annealed Si_D distributions and their annealing behavior now show that these distributions are located at the end region of the H range beyond the maximum value of the deposited energy, and also beyond the maximum concentration of the H distribution. We observe, furthermore, that in the region of the deposited energy peak of the as-implanted sample, the vacancies associated with SiH centers increase the lattice relaxation caused by H atoms, and hence reduce the number of Si_D atoms, which would be produced as a result of the presence of H impurities. This mechanism can be expected to enhance the epitaxial crystallization of Si induced by the ion beam.[31]

As illustrated in Fig. 7, the total amount of H retained in the 35-keV sample stays constant during the annealing between 300 and 600 K, although the H profile becomes narrower. The mobile H is trapped in the region with the maximum H concentration, presumably by the H-induced dislocation loops.[2] In the cases of the 60- and 100-keV samples, where a continuous loss of H is observed (Fig. 1), the evolutions of the Si_D distributions (Fig. 2) indicate the trapping of mobile H in the region beyond the maximum of the deposited energy distribution. In the case of the 35-keV sample, the evolution of the maximum H and Si_D atom concentrations around the modal H range at 450 nm shows that the defect caused by one H atom corresponds effectively to that of about ten Si_D atoms. The same ratio is also observed in the an-

TABLE I. Analyzed vacancy distributions in H^+-implanted and annealed Si(100) samples. The dose in all the samples is 1×10^{16} H/cm^2.

Implantation energy (keV)	Annealing temperature (K)	Divacancy concentration (10^{19} cm^{-3})	Depth of defective surface layer (nm)
35	as-implanted	3.9	100
	570	0.16	500
	720	1.18	500
	970	0.05	800
60	as-implanted	1.5	400
	570	0.06	1500
	720	0.05	2000
	970	0.02	2000
100	as-implanted	0.7	800
	570	0.4	450
	720	0.05	1500
	970	0.02	1500

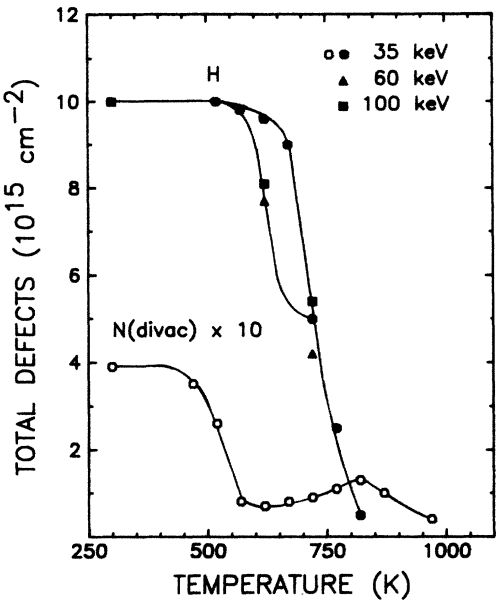

FIG. 7. Amounts of retained H and total number of vacancies vs annealing temperature.

nealed 60- and 100-keV samples. This is further evidence that the number of Si_D atoms is associated with the H concentration in the lattice rather than with the damage caused by the deposited energy. According to the modified Kinchin-Pease model,[32,33] the number of Si_D atoms should be about 5×10^{21} Si_D/cm^3, calculated for the fluence 10^{16} H^+-ions/cm^2, the deposited energy 0.25 eV/Å, and the threshold displacement energy 20–30 eV for creating a permanent Frenkel pair.[34–36] The observed increase in the ratio 10:1 of Si_D to H atoms occurring above 650 K is explained by the fact that the damage is removed by the solid-phase epitaxial growth at temperatures 800–900 K (Ref. 37) after the loss of H at 650–850 K.

IV. COMPUTER SIMULATIONS AND DISCUSSION

We have performed computer simulations to understand further the production of damage during the H implantation. The collision cascades were calculated using the binary collision lattice simulation code COSIPO.[38]

As the principles of the simulation have already been described,[38] only the main parameters used in the present work are given.

The electronic stopping power was taken from our earlier study[39]

$$S_e = f_e S_e^{\mathrm{LSS}} / \{1 + 0.002\,35[E(\mathrm{keV})]^{1/2}\} \quad (16)$$

based on the function given by Demond *et al.*[14] $S_e^{\mathrm{LSS}} = kE^{1/2}$ is the LSS-electronic stopping power.[40] The correction factor f_e was adjusted so that the experimental and calculated modal ranges were coincident for each energy. The interatomic potential is a mean of 50 atom-atom potentials calculated from Dirac-Fock electron densities.[41] The root-mean-square vibration amplitude of the uncorrelated thermal vibrations was 0.06 Å. The maximum impact parameter was 1.6 Å.

The structure and orientation of the *c*-Si samples were included in the simulation of the range profiles. The value of 0.6 was used for f_e in order to reproduce range distributions of the H^+ ions in agreement with those measured by NRB. Thus, the deposited energy distribution shown in Fig. 8 is compatible with the experiment.

In the first part of the range, the damage is partly produced in the form of energetic spikes; the energies of primary recoiling Si atoms are up to 4.7, 8.0, and 13.3 keV in the 35-, 60-, and 100-keV implantations, respectively. Isolated Frenkel pairs are produced near the end of the range, i.e., in the peak region of the deposited energy distribution where the energies of primary recoils are below 1 keV. Note that during the slowing down of ions heavier than H, the collisions lead predominantly to the formation of spikes, and the mechanisms associated with the spike model[7] or the critical damage density model[8,9] cannot be separated experimentally. About 4000 histories were calculated, but only some tens of primary recoiling Si atoms with an energy above 2 keV were created. In spite of the low statistics, limited by the very long computing time, the maximum range of the vacancy distribution (very sensitive to the threshold energy) could be determined well.

The experimentally obtained region of the vacancy-type defects in the as-implanted sample were reproduced in the simulations by adapting a threshold energy of 2.0±0.5 keV for the primary recoiling Si atoms to create a stable vacancy defect. The error limits are mainly due to the uncertainty in the width of the experimental vacancy-defect distribution. This value corresponds to the energy needed to produce enough damage to survive the dynamic and room-temperature annealing. The concentrations shown in Fig. 8 illustrate the numbers of created divacancies, and were obtained by using a displacement energy 25 eV (Refs. 34–36) for the recoiling Si atoms to create a permanent Frenkel pair and by dividing the number of deduced vacancies by two.

The concept of the threshold energy explains the failure to produce amorphous Si in a high-fluence 1-MeV e^- irradiation below 10 K.[42] The energies of primary recoiling Si atoms ($\lesssim$150 eV) did not exceed a threshold value. At 10 K, the threshold energy for the production of permanent damage is apparently between 150 eV and 2.0 keV. A somewhat similar threshold energy concept has previously been proposed by Stein *et al.*[25–27] on the basis of B, O, Zn, and Sb implantations of *c*-Si. They explained the results by assuming that an ion energy of 1.5±0.5 keV is spent in atomic processes per unit volume in the formation of a divacancy. Thus they assumed that the critical damage density model is valid. The essential point of the present work is that a suitable choice of the implanted ion and its energy enables us to show that a critical threshold energy is needed, and that a stable divacancy is created only if a sufficiently large disorder is produced locally, i.e., in an energy spike.

In Fig. 9, the damage induced in *c*-Si by H implanta-

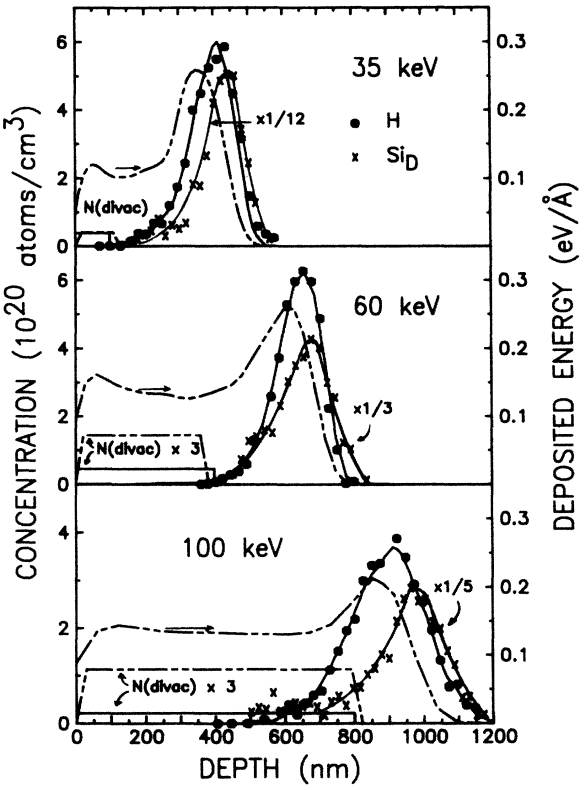

FIG. 8. Hydrogen distributions of the 1×10^{16} 35-, 60-, and 100-keV H^+-ions/cm^2 in *c*-Si (the solid lines through the measured points are the computer simulations of the range profiles) along with the measured displaced Si atom and divacancy distributions (solid lines). The dashed lines close to the H distributions show the corresponding distributions of the deposited energy caused by the nuclear energy loss. The vacancy distributions simulated using collision-cascade calculations are represented by the dashed lines.

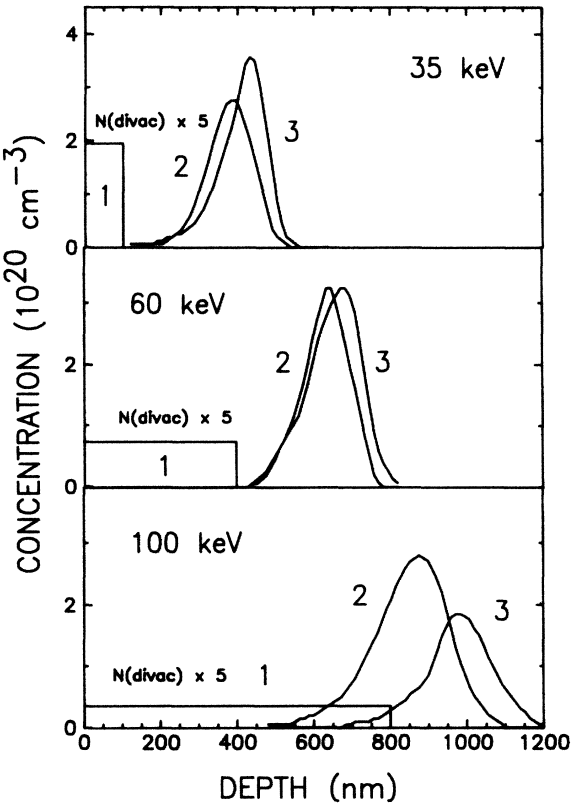

FIG. 9. Defect distributions in H-implanted *c*-Si. The numbers given refer to the three different regions observed. The H-trap distributions of the as-implanted samples used in the Monte Carlo simulation are given by 2 and 3.

tion is shown to be concentrated on three different regions: (1) the region of vacancy-type defects (divacancies) ranging from 0 to 100, 400, and 800 nm for the 35-, 60-, and 100-keV samples, respectively, (2) the region where the H profile and deposited energy distribution overlap and where vacancies are associated with the SiH centers, and (3) the region behind the modal ranges at around 400 (35 keV), 800 (60 keV), and 1000 nm (100 keV) where the damage is produced by the H concentration and appears as Si_D concentrations.

At about 600 K, detrapping of H atoms from the region of the SiH-vacancy centers is observed in all the samples. In the 35-keV sample, the mobile H is trapped in the region with the maximum H concentration. In the 60- and 100-keV samples, H diffuses predominantly to the surface. H atoms detrapped from the type-2 damage region and trapped in the type-3 damage region can be seen by the increase of Si_D atoms in the type-3 damage region (Fig. 2). The difference in the H loss of the 35-keV samples and that of the 60- and 100-keV samples is obviously due to the decrease in the type-3 damage region relative to the type-2 damage region and to the fact that the divacancy region bridges the H concentration profile and the surface of the 60- and 100-keV samples. At annealing temperatures above 700 K, a gradual H loss is observed in all the samples.

In order to obtain approximate recovery energies for the damage of types 2 and 3, the annealing behavior of H-concentration profiles was simulated by a simple model based on Monte Carlo calculations.[43] The distribution of H in the SiH-vacancy region (type-2 damage) was approximated by the overlap of the calculated deposited energy profile and the measured as-implanted H profile. The distribution of H not affected by the SiH-vacancy centers was assumed to be the difference between the original H concentration distribution and that of type-2 traps. The fitting parameters to reproduce the experimental annealing behavior were the recovery energies E_2 and E_3 and also the scaling factor determining the relative amount of H in type-2 and type-3 traps.

A detailed description of the computer simulation is given in Ref. 43. This simple model was modified to take into account the lack of homogeneity of the samples. In the 35-keV sample, *c*-Si on both sides of the H profile was assumed to be a diffusion barrier below 620 K, where the loss of H begins to occur. The retrapping of H atoms released from traps of type 2 (around 570 K) was assumed to be proportional to the concentration of H in traps of type 3. In the 60- and 100-keV samples, no

diffusion barrier between the surface and H profile was needed. The simulation of the annealed H profiles shown in Fig. 1 yielded the energies $E_2 = 1.7$ eV and $E_3 = 2.1$ eV. Figure 9 shows how the number of traps of type 2, (SiH-vacancy complexes) increases with the increasing implantation energy.

The present results show that after a room-temperature H implantation of *c*-Si, there are three different regions of damage (Fig. 9) which survive the dynamic and room-temperature annealing. The accumulation of damage in H-implanted *c*-Si cannot be predicted realistically by focusing attention on the distribution of the deposited energy.[6] Only in the region of the type-2 traps can the dependence of the damage formation on the deposited energy be anticipated.

V. CONCLUSIONS

We have combined the distribution measurements of H and Si_D atoms with those of vacancy-type defects in H-implanted *c*-Si and obtained direct evidence which shows the following.

(i) There are three different damage regions which do not correlate with the deposited energy distribution.

(ii) A threshold energy of 2.0±0.5 keV is needed for primary Si recoils for the production of a vacancy-type damage region which survives the dynamic and room-temperature annealing.

(iii) In the region of the deposited energy peak H is associated with damage consisting of SiH centers and vacancy complexes. Vacancies reduce the number of Si_D atoms which would be produced by H impurities.

(iv) At the end region of the range, H impurities in *c*-Si produce Si_D atoms and affect the solid phase epitaxial growth of damaged *c*-Si.

ACKNOWLEDGMENT

This work has been supported by the Academy of Finland.

[1]S. T. Picraux, F. L. Vook, and H. J. Stein, in *Proceedings of the International Conference on Defects and Radiation Effects in Semiconductors, Nice, France, 1978,* edited by J. H. Albany (Institute of Physics, Bristol, England, 1979), p. 31.

[2]J. W. Corbett, J. K. Karins, and T. Y. Tan, Nucl. Instrum. Methods **182&183**, 457 (1981).

[3]W. R. Brown, in *Beam-Solid Interactions and Phase Transformations,* MRS Symposium Proceedings edited by H. Kurz, G. L. Oesan, and J. M. Poate (Materials Research Society, Pittsburgh, 1985), Vol. 51, p. 53.

[4]J. S. Williams, in *Beam-Solid Interactions and Phase Transformations,* Ref. 3, p. 83.

[5]W. J. Choyke, R. B. Irwin, J. N. McGruer, J. R. Townsend, K. Q. Xia, N. J. Doyle, B. O. Hall, J. A. Spitznagel, and S. Wood, in *Proceedings of the 13th International Conference on Defects in Semiconductors, Coronado, California, 1984,* edited by L. C. Kimerling, and J. M. Porsey, Jr. (American Institute of Metallurgical Engineers, Warendale, 1984), p. 789.

[6]B. O. Hall, Nucl. Instrum. Methods B **16**, 177 (1986).

[7]J. A. Davies, in *Ion Implantation and Beam Processing,* edited by J. S. Williams and J. M. Poate (Academic, Sydney, 1984), Chap. 2.

[8]L. A. Christel, J. F. Gibbons, and T. W. Sigman, J. Appl. Phys. **52**, 7143 (1981).

[9]M. L. Swanson, J. R. Parsons, and C. W. Hoelke, Radiat. Eff. **9**, 249 (1971).

[10]J. Keinonen, M. Hautala, E. Rauhala, M. Erola, J. Lahtinen, H. Huomo, A. Vehanen, and P. Hautojärvi, Phys. Rev. B **36**, 1344 (1987).

[11]H. J. Whitlow, J. Keinonen, M. Hautala, and A. Hautojärvi, Nucl. Instrum. Methods B **5**, 505 (1984).

[12]J. Lahtinen, A. Vehanen, H. Huomo, J. Mäkinen, P. Huttunen, K. Rytsölä, M. D. Bentzon, and P. Hautojärvi, Nucl. Instrum. Methods **B17**, 73 (1986).

[13]J. F. Ziegler *et al.*, Nucl. Instrum. Methods **149**, 19 (1978).

[14]F.-J. Demond, S. Kalbitzer, J. Mannsperger, and G. Müller, Nucl. Instrum. Methods **168**, 69 (1980).

[15]H. H. Andersen and J. F. Ziegler, *The Stopping and Ranges of Ions in Matter* (Pergamon, New York, 1977), Vol. 3.

[16]L. C. Feldman, J. W. Mayer, and S. T. Picraux, *Materials Analysis by Ion Channeling* (Academic, New York, 1982); W. K. Chu, J. W. Mayer, and M.-A. Nicolet, *Backscattering Spectrometry* (Academic, New York, 1978).

[17]J. F. Ziegler, *The Stopping and Ranges of Ions in Matter* (Pergamon, New York, 1977), Vol. 4.

[18]*Positron Solid State Physics,* edited by W. Brandt and A. Dupasquier (North-Holland, Amsterdam, 1983).

[19]J. Mäkinen, A. Vehanen, P. Hautojärvi, H. Huomo, J. Lahtinen, R. M. Nieminen, and S. Valkealahti, Surf. Sci. **175**, 385 (1986); M. D. Bentzon, H. Huomo, A. Vehanen, P. Hautojärvi, J. Lahtinen, and M. Hautala, J. Phys. F **17**, 1477 (1987).

[20]K. G. Lynn, D. M. Chen, B. Nielsen, R. Pareja, and S. Myers, Phys. Rev. B **34**, 1449 (1986).

[21]A. Vehanen, K. Saarinen, P. Hautojärvi and H. Huomo, Phys. Rev. B **35**, 4606 (1987).

[22]B. Nielsen, K. G. Lynn, A. Vehanen, and P. J. Schultz, Phys. Rev. B **32**, 2296 (1985).

[23]E. Punkka, A. Vehanen, P. Hautojärvi, J. Keinonen, E. Rauhala, and M. Hautala (unpublished).

[24]S. Dannefaer, G. W. Dean, D. P. Kerr, and B. G. Hogg, Phys. Rev. B **14**, 2709 (1976).

[25]H. J. Stein, F. L. Vook, and J. A. Borders, Appl. Phys. Lett. **16**, 106 (1970).

[26]H. J. Stein, and W. Beezhold, Appl. Phys. Lett. **17**, 442 (1970).

[27]H. J. Stein, F. L. Vook, D. K. Brice, J. A. Borders, and S. T. Picraux, Radiat. Eff. **6**, 19 (1970).

[28]W. Mayer, D. Grasse, and J. Peisl, Radiat. Eff. **84**, 107 (1985).

[29]H. J. Stein, Phys. Rev. Lett. **43**, 1030 (1979).

[30]W. K. Chu, R. H. Kastl, R. F. Lever, S. Mader, and B. Masters, Phys. Rev. B **16**, 3851 (1977).

[31]R. G. Elliman, S. T. Johnson, A. P. Pogany, and J. S. Williams, Nucl. Instrum. Methods B **7&8**, 310 (1985).

[32]P. Sigmund, Radiat. Eff. **1**, 151 (1969).

[33]M. J. Norgett, M. T. Robinson, and I. M. Torrens, Nucl. Eng. Des. **33**, 50 (1974).

[34]P. Sigmund, Appl. Phys. A **30**, 43 (1983).

[35]S. Matteson, B. M. Paine, and M.-A. Nicolet, Nucl. Instrum.

Methods **182&183**, 53 (1981).
[36]J. Bøttiger, S. K. Nielsen, and P. Thorsen, Nucl. Instrum. Methods B **7&8**, 707 (1985).
[37]L. Csepregi, J. W. Mayer, and T. W. Sigman, Phys. Lett. **54A**, 157 (1975).
[38]M. Hautala, Phys. Rev. B **30**, 5010 (1984).
[39]M. Hautala, J. Keinonen, H. J. Whitlow, P. Tikkanen, M. Uhrmacher, and K. P. Lieb, Phys. Lett. **109A**, 344 (1985).
[40]J. Lindhard, M. Scharff, and N. E. Schiøtt, K. Dan. Vidensk. Selsk. Mat.-Fys. Medd. **33**, No. 14 (1963).
[41]M. Bister, M. Hautala, and M. Jäntti, Radiat. Eff. **42**, 201 (1979).
[42]D. N. Seidman, R. S. Averback, P. R. Okamoto, and A. C. Baily, Phys. Rev. Lett. **58**, 900 (1987).
[43]J. Keinonen, V. Karttunen, J. Räisänen, F.-J. Bergmeister, A. Luukkainen, and P. Tikkanen, Phys. Rev. B **34**, 8981 (1986).